ACS APPLIED MATERIALS & INTERFACES

Research Article

www.acsami.org

Alginic Acid Nanoparticles Prepared through Counterion Complexation Method as a Drug Delivery System

Yuan Cheng, Shuling Yu, Xu Zhen, Xin Wang, Wei Wu, and Xiqun Jiang*

Laboratory of Mesoscopic Chemistry and Department of Polymer Science & Engineering, College of Chemistry & Chemical Engineering, Nanjing University, Nanjing 210093, P. R. China

ABSTRACT: In this paper, a kind of novel alginic acid nanoparticles was successfully prepared by a non-solvent-aided counterion complexation between anionic alginic acid and cationic 2,2′-(ethylenedioxy)diethylamine in aqueous solution followed by cross-linking alginic acid moiety using Ca^{2+}. It was found that these alginic acid nanoparticles have a spherical morphology with the diameter of about 100 nm, and negatively charged surface with the zeta potential of about −30 mV. Compared to the desintegrity of un-cross-linked nanoparticles, the Ca^{2+}-cross-linked nanoparticles maintained their integrity in the aqueous medium with the physiological pH value. Doxorubicin, a model antitumor drug, was successfully loaded into the alginic acid nanoparticles, and their in vitro and in vivo antitumor activities were evaluated. It was found that these negatively charged nanoparticles could be taken up by the cancer cells through an endocytosis mechanism. In vivo near-infrared (NIR) fluorescence imaging and biodistribution examinations showed that the alginic acid nanoparticles could be well-accumulated in the tumor site by the enhanced permeability and retention effect. In vivo antitumor examination showed that the drug-loaded nanoparticles have superior efficacy in impeding tumor growth and prolonging the lifetime of H22 tumor-bearing mice than free drug.

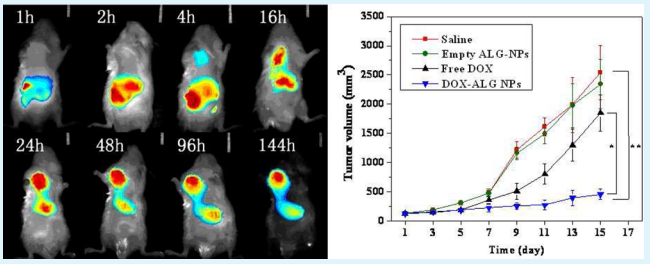

KEYWORDS: *alginic acid, nanoparticles, drug delivery, antitumor, doxorubicin*

INTRODUCTION

For chemotherapeutic purposes, biocompatible and biodegradable polymeric nanoparticles (NPs) have been designed and developed rapidly over the past two decades.[1−5] These NPs could be employed as effective antitumor drug carriers to control drug release. Meanwhile, the circulation time of the loaded drug could be significantly prolonged compared to that of free drug, which is beneficial for antitumor therapy.[6−9] Furthermore, the NPs could accumulate in solid tumors in passively and actively targeting fashions by leaky blood vessels in tumor sites and targeting groups on the nanoparticle surface.[10−13] Thus, the development of novel nanoparticulate drug delivery systems that are safe and effective in vivo is highly desirable.

Alginic acid (ALG) is a linear anionic polysaccharide consists of α-L-guluronic acid and β-D-mannuronic acid, and generally regarded as safe by the U.S. Food and Drug Administration.[14−18] Because of its biocompatible, biodegradable and mild gelation properties, ALG has been widely used in a variety of biomedical applications. For example, ALG hydrogels could act as protein and drug delivery systems.[19,20] ALG hydrogels were also used as scaffold materials for the microencapsulation of a range of different living cells for therapeutic applications and tissue engineering.[21,22] In contrast to ALG hydrogels, the investigation in ALG-based nanoparticulate drug delivery systems is limited despite the fact that some advances have been made in the preparation of alginate-based micro- and submicrometer particles. For instance, by taking advantage of the gelation property of ALG by bivalent metal cations, alginate in aqueous solution is initially pregelled by Ca^{2+}, and then the aggregates of alginate molecules in the pregel state are electrostatically complexed with positively charged polyelectrolytes added such as poly-L-lysine, chitosan, and polyethylenimine to form the nanoparticles.[23−25] Thus, these nanoparticles are enveloped by cationic polyelectrolyte and were used for drug delivery.[24−26] More recently, the preparation of 350 nm sized alginate NPs through microemulsion method was reported.[27] Differently, in our previous work, ALG NPs were successfully prepared in complete aqueous medium by polymerizing cationic 2-(diethylamino)ethyl methacrylate in the presence of alginic acid. These alginic acid nanoparticles are monodispersed in size and have negatively charged surface.[28] The abundant carboxyl groups at the surface of the alginic acid NPs ensures that these NPs have a negatively charged surface in blood circulation, and feasible to escape from the adsorption and capture of negatively charged protein in physiological conditions.[29−31]

Doxorubicin (DOX) is an anticancer agent of broad spectrum and widely used for the treatment of various cancers such as breast, prostate, brain, and lung cancers.[6] However,

Received: July 8, 2012
Accepted: September 28, 2012
Published: September 28, 2012

   dx.doi.org/10.1021/am3012627 | *ACS Appl. Mater. Interfaces* 2012, 4, 5325−5332

DOX also has a strong cytotoxic action to normal tissues. To decrease the toxic side effects, loading DOX into nanoparticles is a promising solution.[7]

In present work, we developed a new strategy to prepare ALG NPs with the diameter of about 100 nm. The small molecule 2,2′-(ethylenedioxy)diethylamine (DA) was initially employed as a building block to electrostatically complex with ALG in aqueous solution to form ALG-DA NPs. After ALG moiety in the NPs was cross-linked by Ca^{2+}, the small molecule DA was partially removed from the NPs by dialysis. These alginic acid-forming NPs were further served as drug carrier and their drug delivery behavior with DOX as a model drug was investigated. After examinations of in vitro cytotoxicity, cellular uptake, *in vivo* near-infrared fluorescence imaging, and in vivo antitumor activity in a model of murine hepatocellular carcinoma (H22), it is found that DOX-loaded ALG NPs exhibit significantly superior antitumor activity compared to free DOX in a murine hepatoma H22 cancer model.

MATERIALS AND METHODS

Materials. Sodium alginate (Beijing Stock of China Medicine Company, 95%) with a viscous-average molecular weight of 170 kDa and a molar fraction of guluronic acid residues of 0.65 was refined by dissolving it in distilled water followed by precipitating with ethanol. 2,2′-(ethylenedioxy)diethylamine (DA), 4′,6-diamidino-2-phenylindole (DAPI), and 3-(4,5-dimethylthiazol-2-yl)-2,5-diphenyltetrazolium bromide (MTT) were purchased from Aldrich. Doxorubicin hydrochloride (DOX) was bought from Shenzhen Main Luck Pharmaceuticals Incorporation. Rhodamine B isothiocyanate and NIR-797 isothiocyanate were bought from Aldrich and Acros, respectively. All other reagents were of analytical grade and used without further purification. Human neuroblastoma cell line, SH_SY5Y cells, and murine hepatic carcinoma cell line, H22, were purchased from Shanghai Institute of Cell Biology. Male Institute of Cancer Research (ICR) mice (6−8 weeks old) were purchased from Animal Center of Nanjing Drum-Tower Hospital.

Preparation of the ALG NPs. Sodium alginate was acidified with 0.1 M HCl and the alginic acid generated was washed with deionized water to remove residue ions. Then, 0.05 g of the resultant alginic acid was dissolved by 0.01 g of DA in 15 mL of distilled water. After 10 mL acetone (nonsolvent) dropwise added into the system with magnetic stirring, the clear solution turned opalescent when the concentration of acetone exceeded a critical value of 26% (v/v), implying the formation of colloidal particles. Next, the resultant suspension was filtered with filter paper to remove any larger aggregate, and dialyzed against acetone solution (40% v/v) containing 0.01 g $CaSO_4$ for 4 h using a dialysis bag (14 kDa cut off) to perform the cross-linking reaction of the ALG NPs. Finally, the cross-linked ALG NPs were again dialyzed against distilled water for 72 h to eliminate small molecules including DA and acetone for further characterization and experiments.

Characterization of the ALG NPs. The morphology of ALG NPs was investigated by transmission electron microscopy (TEM, JEM-100S, JEOL, Japan). For the TEM observation, properly diluted samples were dropped onto a copper grid covered with a nitrocellulose membrane and air-dried without any staining.

Mean diameter and size distribution of ALG NPs in the aqueous medium were determined by dynamic light scattering (DLS) method using a Brookhaven BI 9000AT system (Brookhaven Instruments Corporation, US). All DLS measurements were done with a laser wavelength of 633.0 nm at 25 °C with a detection angle of 90°.

Zeta potential of ALG NPs was measured with Zetaplus (Brookhaven Instruments Corporation, US) at room temperature. Each sample of the NPs was adjusted to a concentration of 0.01 g/mL in distilled water in the case of zeta potential examination. All analyses were triplicate and the results were the average of three runs.

^{1}H NMR measurement of ALG NPs was performed with Bruker DRX 500 (Bruker, Germany) in D_2O. In comparison, the ^{1}H NMR spectra of sodium alginate was also obtained in D_2O.

Element analysis of ALG NPs and sodium alginate was carried out on Vario EL II element analyzer (Elementar, Germany). The samples were dried in vacuum at 40 °C for 48 h and the results were the average of three runs.

Preparation of Doxorubicin-Loaded ALG NPs (DOX-ALG NPs). To the predetermined ALG NPs aqueous solution (pH 7.4), 5 mg/mL of DOX solution was added dropwise with magnetic stirring to make sure that the weight ratio of DOX to ALG NPs is 0.25, and the solution were ultrasonically dispersed for 5 min and placed in the darkness with constant stirring at 37 °C for 72 h, and then filtered with filtering membrane with pore size of 220 nm to remove any precipitate. The residual free DOX in the prepared DOX-ALG NPs suspension was removed by centrifugation at 15 000 rpm for 30 min, and the sediment, i.e., DOX-ALG NPs, was redispersed in distilled water for further use.

DOX Loading Content and Encapsulation Efficiency. For the measurement of DOX loading content and encapsulation efficiency, the prepared DOX-ALG NPs was centrifuged and the sediment was dried in vacuum at 40 °C for 48 h, and weighed. Free DOX in supernatant was measured by SHIMADZU UV 2401 spectrometer (Shimadzu, Japan). DOX loading content and encapsulation efficiency were calculated by equations as follows.

$$\text{DOX loading content (\%)} = \frac{\text{weight of DOX in nanoparticles}}{\text{weight of the nanoparticles}} \times 100\%$$

$$\text{encapsulation efficiency (\%)} = \frac{\text{weight of DOX in nanoparticles}}{\text{weight of the feeding DOX}} \times 100\%$$

In vitro Release of the DOX-ALG NPs. One milliliter of aqueous solution of the DOX-ALG NPs was placed into a preswelled dialysis bag (14 kDa cut off) and then immersed into 3 mL of 0.01 M phosphate-buffered saline (PBS). This release system was adjusted with PBS to pH 5.0, 5.5, 6.0, and 7.4, respectively, and gentle agitated at 37 °C in the darkness. Periodically, 3 mL of release medium was withdrawn and then 3 mL of fresh PBS was added to the system. The DOX concentration in the sampled medium was determined by UV spectrometer with absorption at wavelength of 490 nm and reference to a calibration curve. All measurements were performed in triplicate.

Cellular Uptake of ALG NPs. For labeling ALG NPs with dye, 1 mg of Rhodamine B isothiocyanate was dissolved in 1 mL of DMSO, and then dropwise introduced into 10 mL of sodium alginate solution. The mixture was magnetically stirred at room temperature for 24 h in the darkness, and precipitated with 100 mL of ethanol. The sediment was redissolved in 10 mL of distilled water and dialyzed with dialysis bag (14 kDa cut off) against distilled water in the darkness for 72 h to remove unreacted Rhodamine B isothiocyanate. The resultant Rhodamine B labeled sodium alginate was acidified and used to prepare Rhodamine B-labeled ALG NPs for the cell uptake experiment. For cellular uptake, 200 μL of Rhodamine B-labeled ALG NPs was added into cell culture medium in 6-well plate with a density of 5000 cells per well and incubated for 2 h at 37 °C in the incubator. In comparison, another sample of 200 μL of Rhodamine B-labeled ALG NPs was stored in the refrigerator together with a 6-well plate that contained 5000 cells per well at 4 °C for 4 h to keep the temperature constant, and then the cooled sample was added into the 6-well plate to conduct cell uptake experiment for 2 h at 4 °C. After incubation, the cells were washed with PBS solution and fixed with 4% (w/v) formaldehyde solution for 30 min, then the fixed cells were washed two times with PBS and distilled water, respectively. DAPI was employed to dye nucleus zone of the cell. The cell uptake images were recorded with confocal laser scanning microscopy (CLSM, LSM 710, Zeiss, Germany).

In vitro Cytotoxicity of DOX-ALG NPs. The cytotoxicities of the DOX-ALG NPs against human neuroblastoma SH_SY5Y cell line were evaluated using MTT assay in comparison of empty ALG NPs and free DOX. The cells were seeded to 96-well plate to ensure 5000 cells per well and then coincubated with various concentrations of empty ALG NPs, free DOX, and the DOX-ALG NPs at 37 °C for 24 h. Next, the medium in each well was removed and 10 μL of MTT assay and 90 μL of fresh medium were then added to the wells. After incubation for 4 h, the solution was removed, leaving the precipitate. 100 μL of dimethylsulfoxide (DMSO) was then added to each well. After 15 min, the cell viability was measured by a microplate reader (GENios, Australia) and determined by the following equation, where I_{sample} and $I_{control}$ represent the magnitude of intensity determined for cells treated with different samples and for control cells (untreated), respectively.

$$\text{cell viability (\%)} = \frac{I_{sample}}{I_{conctrol}} \times 100\%$$

NIR Fluorescence Labeling and In vivo Imaging. One milligram of NIR-797 isothiocyanate was dissolved in 1 mL of DMSO and dropwise introduced into 10 mL of aqueous solution of the ALG NPs. The mixture was magnetically stirred at room temperature for 24 h in the darkness, and then dialyzed against distilled water for 72 h to remove unreacted NIR-797 isothiocyanate.

All the animal experiments were reviewed and approved by Animal Care and Use Committee, Nanjing University. 5×10^5 murine H22 cells in 0.1 mL saline were subcutaneously inoculated into the right limb armpits of one ICR male mice. The mouse was kept 7 days with free access to food and water. After that, 0.2 mL of NIR-797 labeled ALG NPs was intravenous (i.v.) injected into the mouse, and the NIR fluorescence images were acquired with Maestro in vivo imaging system (CRi, USA) on predetermined times.

In vivo Antitumor Activity. H22 bearing ICR mice (average body weight of 25 g) described above were randomly divided into 4 groups (10 mice per group). After the mice were allowed to free access food and water for 7 days, saline, empty ALG NPs, free DOX at the dose of 4 mg of DOX/kg of body weight (4 mg/kg), DOX-ALG NPs at the dose of 4 mg/kg DOX eq. were i.v. injected via a tail vein, respectively. The tumor volume was measured every other day using calipers for 15 days. The tumor volume was calculated using the following equation.

$$\text{tumor volume (mm}^3\text{)} = \frac{1}{2} \times \text{length} \times \text{width}^2$$

Biodistribution of DOX in Mice. For the biodistribution study, the H22 tumor-bearing ICR mice as described above were randomly divided into 7 groups (3 mice per group). The mice (25 g in average) of 6 groups were i.v. injected with DOX-ALG NPs at a dose of 4 mg/kg DOX eq., leaving a group as a blank group. At a predetermined time after the i.v. injection, the mice were sacrificed and their blood, heart, liver, spleen, lung, kidney and tumor were collected immediately. The blood was centrifuged at 15000 rpm for 30 min, and 100 μL supernatant was diluted to 3 mL with 60% alcohol and 5% hydrochloric acid aqueous solution. The tumors and organs were weighed and homogenized with 60% alcohol and 5% hydrochloric acid aqueous solution. After centrifugation at 15 000 rpm for 30 min, the supernatant of the homogenized tissue was also diluted to 3 mL with 60% alcohol and 5% hydrochloric acid aqueous solution. The DOX concentration in the homogenized tissue was measured using a SHIMADZU 5300 UV–Vis spectrophotometer (Shimadzu, Japan). The measured average values of each tissue from the blank group were served as background and deducted from corresponding sample of the administrated mice. The biodistribution for free DOX was done with the same procedure described above in comparison.

Statistical Analysis. Student's *t* test was employed to determine the difference of tumor inhibition between the groups treated with the DOX-loaded ALG NPs and free DOX, and *P* values less than 0.05 were considered statistically significant.

RESULTS AND DISCUSSION

Preparation of the ALG NPs. In present work, the ALG NPs were prepared by a nonsolvent-aided counterion complexation between cationic DA and anionic ALG in aqueous solution, as shown in Scheme 1. Initially, the water-insoluble

Scheme 1. Schematic Illustration of the Preparation of ALG NPs

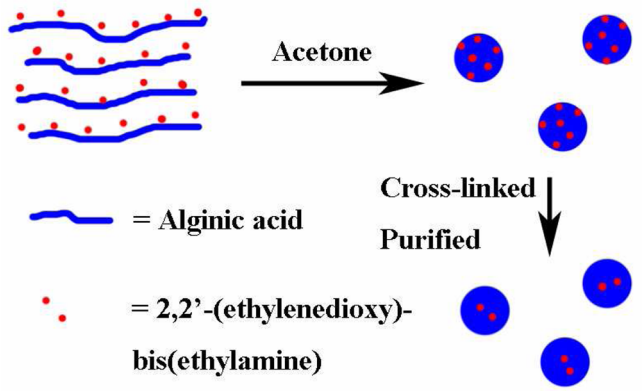

ALG was well dissolved in water in the help of DA due to formation of acid–base ion pair. Then, acetone, a nonsolvent for both ALG and DA, was added into the system. This may make ALG chains and DA molecules to get closer, resulting in increased counterion interactions and the assembly of ALG and DA into colloidal particles. When acetone added reaches to some extent in the system, the clear solution of the system turns opalescent, suggesting the formation of colloidal particles. Finally, the ALG-DA colloidal suspension was dialyzed against the aqueous medium with the same acetone concentration to keep the ALG-DA NPs stable. Meanwhile, $CaSO_4$ was added to the medium to gel the ALG.[32] Because $CaSO_4$ has a low ionization degree in water, it can release Ca^{2+} into aqueous solution in a thin and steady pattern, which is very helpful to the cross-linking of ALG. Thus, the ALG moiety in ALG-DA NPs was gradually gelled by Ca^{2+} which diffused into the dialysis bag. The resultant ALG NPs were again dialyzed against distilled water to remove DA, acetone and other small molecules.

In addition, it is necessary to utilize the form of the alginic acid (ALG) not alginate since the alginate itself has already ionized and there is no enough interaction between the alginate and DA. The proof is, when the ALG was changed into sodium alginate, no nanoparticle appeared but only sediment under the same procedure. The diameters of the uncross-linked ALG NPs at different weight ratio of DA to ALG were summarized in Table 1. From Table 1, it can be seen that when the weight ratio of DA to ALG is 0.2, the ALG NPs receive most narrow

Table 1. Size of the ALG NPs at Different Weight Ratios of ALG to DA[a]

weight ratio of DA and ALG	diameter (nm)	polydispersity index	scatter intensity (Mcps)
0.15	307 ± 16	0.176	2.0
0.20	248 ± 9	0.169	3.3
0.30	185 ± 1	0.208	1.4

[a]The measurements were carried out in 40% (v/v) acetone solution at pH 5.0, and the ALG NPs were not cross-linked.

dx.doi.org/10.1021/am3012627 | ACS Appl. Mater. Interfaces 2012, 4, 5325–5332

distribution, and the light scatter intensity of the ALG NPs is the highest in all tested samples, indicating that the yield of ALG NPs is highest under this ratio. Although the rise of the ratio of DA to ALG can decrease the diameter of the ALG NPs, as shown in Table 1, the polydispersity index increases, and the sample becomes not very stable. Therefore, to achieve a good balance between the dispersing stability and the diameter, in subsequent experiments, the weight ratio of DA to ALG was chosen to be 0.2 to prepare ALG NPs. Besides, the concentration of acetone and cross-linking time are both optimized to prepare size-desired and pH stable ALG NPs.

Characterization of ALG NPs. The size and morphology of ALG NPs were investigated by DLS in aqueous solution and by TEM in solid state. Figure 1a shows the size distribution of

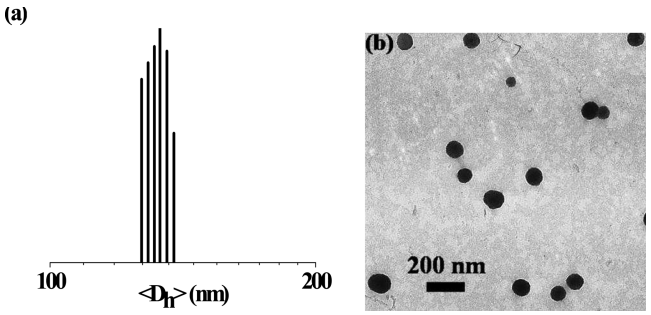

Figure 1. (a) Hydrodynamic diameter distribution measured by DLS, and (b) TEM image of the ALG NPs at pH 7.4.

prepared ALG NPs measured by DLS at pH 7.4. It can be seen that the sample displays a narrow unimodal size distribution with mean hydrodynamic diameter (D_h) of 132 ± 6 nm. Compared to that of uncross-linked particles in Table 1, the size of Ca^{2+}-cross-linked ALG particles decreases significantly. Typical TEM image of the ALG NPs is shown in Figure 1b, from which it can be seen that the ALG NPs are solid spheres with the diameter of about 100 nm, which is a little smaller than that of DLS measurement due to dehydration of the sample. Since the ALG NPs were physically cross-linked by Ca^{2+}, the stability of resulting ALG NPs in the medium with different pH values was investigated and the results are presented in Figure 2a. It can be seen that the mean diameter of nanoparticles increases from 94 to 150 nm when the pH value of the medium is changed from 5.5 to 8.0. This may attribute to that with the increase of pH value, and the ALG moiety of the nanoparticles becomes more hydrated and extended because of deprotonation. On the other hand, it can be seen that the light scattering intensity of the sample changes little when medium's pH increases from 5.5 to 8.0, suggesting that ALG NPs have the favorable structural stability and endurance against pH change. The zeta potentials of the ALG NPs at different pH values are given in Figure 2b, from which it can be seen that the zeta potential of the ALG NPs is −28 mV to −37 mV in pH range from 5.5 to 8.5, respectively, because the carboxyl groups on the backbone of the ALG are deprotonated. These results indicate that the ALG NPs are pH stable and have negatively charged surface.

The ^{1}H NMR spectra of the ALG NPs and sodium alginate in D_2O are shown in Figure 3. It can be seen that there is hardly difference between the ALG NPs and sodium alginate. No new signal is detected, such as DA, which signal appears around 2.8 ppm and 3.5 ppm, respectively. The spectrum of the ALG NPs in D_2O is corresponded to the shell of the ALG NPs, which is

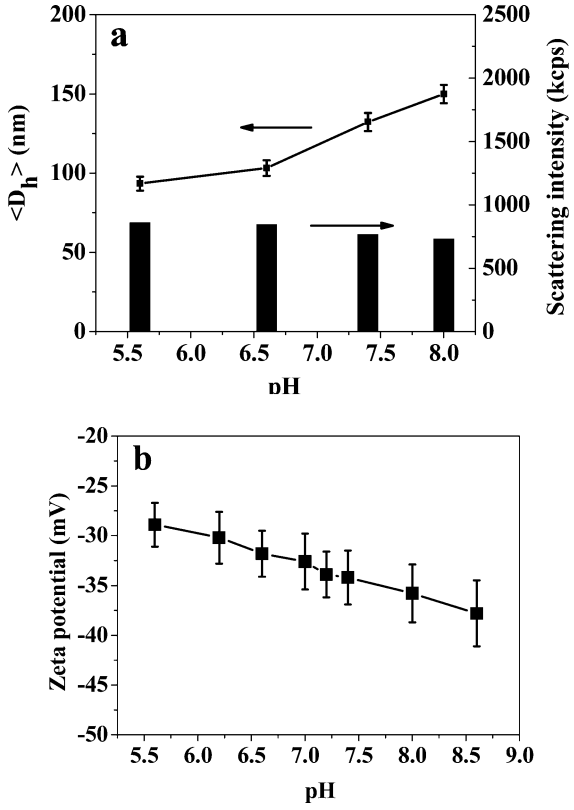

Figure 2. (a) Hydrodynamic diameters and light scattering intensities as a function of pH, and (b) zeta potentials of the ALG NPs at different pH values.

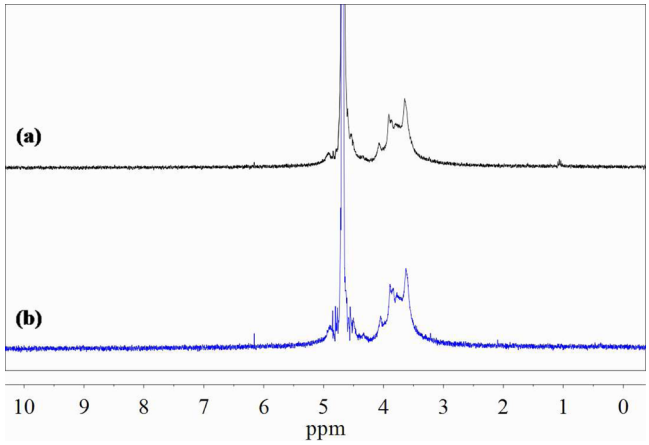

Figure 3. ^{1}H NMR spectra of (a) the ALG NPs and (b) sodium alginate in D_2O.

hydrated by D_2O. This result illustrated that the surface of the ALG NPs is pure ALG. However, it was found that DA could not be eliminated completely after dialysis based on the data of element analysis. The DA content in ALG NPs is about 8.4 wt %, and about 63.4% amount of the DA added into the system is removed after dialysis. The reason why DA could not be removed completely may be ascribed to the complex interaction of the ALG and DA inside the ALG NPs and the impediment of the cross-linked shell of the ALG NPs that hinders the DA diffusion to outside the NPs.

DOX Loading and Release from ALG NPs. Considering that the ALG NPs have abundant carboxyl groups in the ALG

molecules, they seem to be very appropriate to load DOX since the DOX contains an amino group in its structure. Consequently, it is found that the DOX loading content and encapsulation efficiency in the ALG NPs reaches 24.5 ± 0.1% and 95.5 ± 0.1%, respectively, indicating that the ALG NPs are indeed effective DOX loading vehicles.

The *in vitro* DOX release profiles from the DOX-ALG NPs at 37 °C in PBS (0.01M) with different pH values are shown in Figure 4. The inset shows the initial release stage within 24 h.

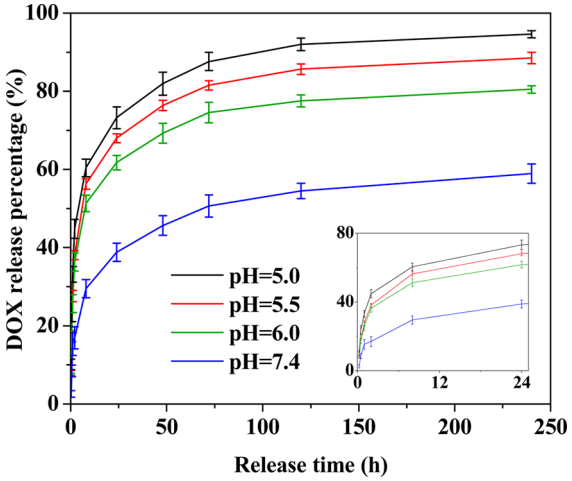

Figure 4. In vitro release profiles of the DOX-ALG NPs at 37 °C in the medium with different pH values.

From Figure 4, it can be seen that DOX release from ALG NPs is pH-dependent and exhibits a steady continued release pattern with a little initial burst release. As pH decreases, DOX release is speeded and the DOX release amount increases. This is due to the protonation of the amino group of the DOX, which increases its solubility. When pH is below 6.0, about 62% of loaded DOX is released from the nanoparticles within 24 h, while about 38.8% of loaded DOX is released at pH 7.4 in the first 24 h. Such pH-sensitive drug release behavior is desirable since the ideal drug release should be slow in the neutral environment of systemic circulation in vivo and relatively faster in the weak acidic environment of tumor tissue.[33−35] Finally, about 59% and 95% of DOX is released from ALG NPs within 240 h at pH 7.4 and 5.0, respectively. These results suggest that ALG NPs are a suitable carrier for DOX loading and release.

Cellular Uptake. To trace the cellular uptake of the ALG NPs, the dye, Rhodamine B, was covalently attached to the backbone of ALG moiety through the reaction with hydroxyl groups of ALG, and then, the Rhodamine B-labeled ALG was used to synthesize dye-labeled ALG NPs as did with nonlabeled ALG. After coincubation of human neuroblastoma SH_SY5Y cells with Rhodamine B-labeled ALG NPs at 37 °C for 2 h, the cell uptake of the NPs was observed by CLSM. Figure 5a shows typical CLMS image of SH_SY5Y cells after incubation with the NPs at 37 °C. It can be seen that a large number of the NPs (red color) are internalized in the cells, and the cells exhibit a diffused distribution of red color in the cytoplasm region. No ALG NP is found in the nucleus region which was stained into blue by DAPI, suggesting that the ALG NPs are unable to penetrate the cell nucleus. In addition, one can see that the SH_SY5Y cells incubated with the NPs still attach well on the glass slide and maintain their normal morphology. This result indicates that even the NPs with negatively charged surface,

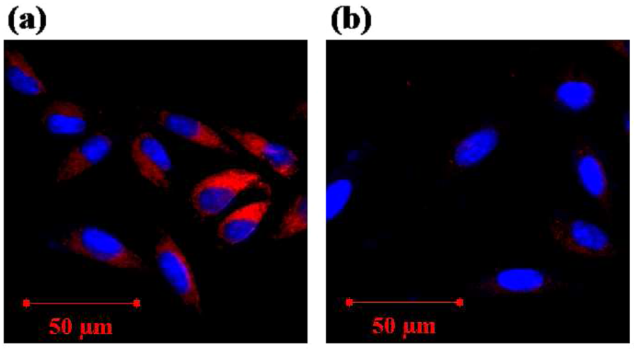

Figure 5. CLSM images of SH_SY5Y cells after incubation with Rhodamine B-labeled ALG NPs for 2 h at (a) 37 °C and (b) 4 °C.

they can still be taken up well by the SH_SY5Y cells. To figure out the cellular uptake mechanism of the ALG NPs, SH_SY5Y cells were coincubated with the dye-labeled ALG NPs at 4 °C for 2 h. Because the lipid bilayer of the cell would be hardened at low temperature, the endocytosis and passive diffusive process would be substantially weakened by lowering temperature.[36] From Figure 5b, it is found that there are hardly ALG NPs inside the cell cytoplasm at 4 °C. Thus, it is believed that the cell uptake of the ALG NPs is mainly caused by endocytosis mechanism.

In vitro Cytotoxicity of DOX-ALG NPs. The in vitro cytotoxicity of the DOX-ALG NPs was evaluated with cultured SH_SY5Y cell line. For comparison, the empty ALG NPs and free DOX were also evaluated. Figure 6 reveals the cytotoxicity

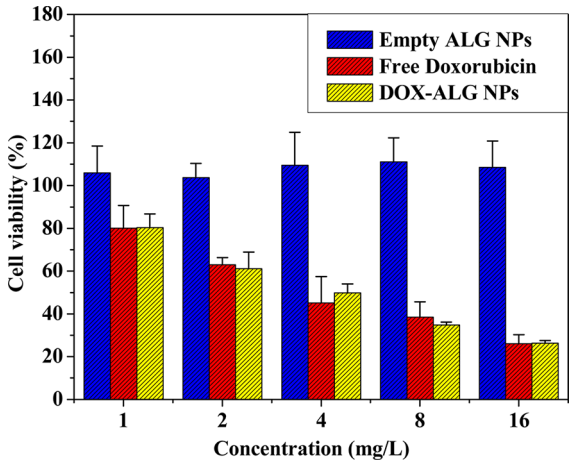

Figure 6. In vitro cytotoxicity of empty ALG NPs, the DOX-ALG NPs, and free DOX against SH_SY5Y cells at 37 °C.

of the objective materials in SH_SY5Y cell line using the MTT assay. From Figure 6, it can be seen that the cell viability of the empty ALG NPs is above 100% within all the testing concentration, meaning that the empty ALG NPs have no toxicity on the SH_SY5Y cell line in the given concentration range. On the other hand, a dose-dependent cytotoxicity is observed for both free DOX and the DOX-ALG NPs. Moreover, the DOX-ALG NPs show similar cytotoxicity to free DOX at equal DOX concentration after 24 h exposure. Considering about 38% and 73% of the loaded DOX being released from ALG NPs in 24 h at pH of 7.4 and 5.0, respectively, the similar cytotoxicity of DOX-ALG NPs to free DOX suggests that the cellular uptake of ALG NPs with

negatively charged surface is more effective than that of free DOX, and the DOX-ALG NPs are efficient drug delivery vehicles.

NIR Fluorescence In vivo Imaging. To investigate the fate of the ALG NPs in a living system, we applied the noninvasive and real-time NIR fluorescence imaging technique to visualize the tissue distribution of ALG NPs in vivo. The ALG NPs were labeled with a NIR fluorescence dye, NIR-797, and then injected into subcutaneous hepatic H22 tumor-bearing mice via a tail vein. Figure 7 displays the in vivo NIR

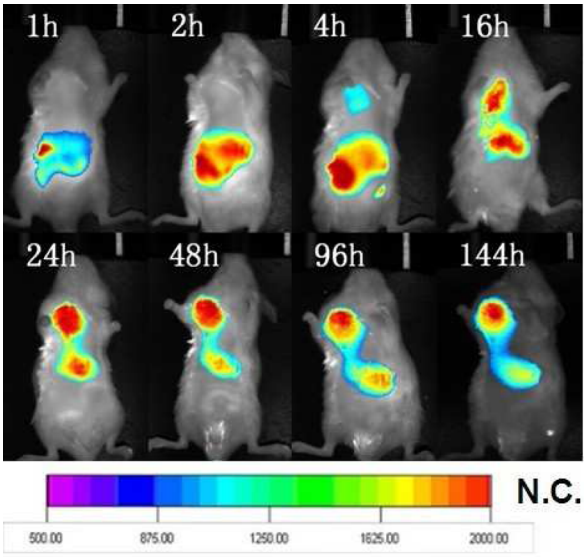

Figure 7. In vivo NIR fluorescence imaging of the H22 tumor-bearing mouse after intravenous injecting NIR-797 labeled ALG NPs.

fluorescence images at different time after injection. The different fluorescence intensities are represented by different colors as shown in color histogram. From Figure 7, it can be seen that the ALG NPs mainly accumulate in liver and intestine in the initial 4 h, indicating that some of the ALG NPs are rapidly recognized by the phagocytic cells and the reticuloendothelial system (RES). After 4 h, the fluorescence signal of the ALG NPs appears in tumor site and becomes stronger and stronger as time escapes. After 16 h, the fluorescence intensity in liver tissue starts to decrease while fluorescence intensity in the tumor region still increases. At 24 h postinjection, the fluorescence intensity in tumor site is already stronger than that in liver. At 144 h postinjection, the ALG NPs left in liver is much less than before, whereas the fluorescence signal in the tumor site is still very strong. These results suggest that a portion of the ALG NPs have the ability to escape from the RES uptake, leading to a long blood circulation time and obvious tumor accumulation.

In vivo Antitumor Activity. The in vivo antitumor activity of the DOX-ALG NPs was evaluated with subcutaneous hepatic H22-bearing mice (10 per group). The treatments were done by i.v. injecting with saline, empty ALG NPs, free DOX (4 mg/kg), the DOX-ALG NPs (4 mg/kg DOX eq.), respectively, into H22 tumor-bearing mice. When the tumor volume of mice grew up to 150 mm^3 in average, they were treated by saline, empty ALG NPs, free DOX, and DOX-ALG NPs, respectively, and this day was designated as Day 1.

Figure 8 shows the variation of tumor volume with time (day) after H22 tumor-bearing mice were treated. It can be

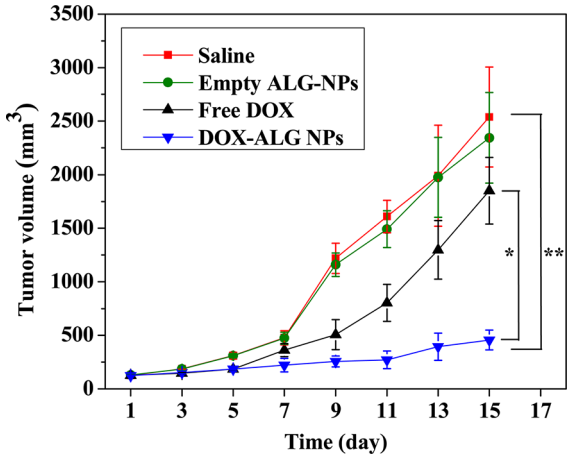

Figure 8. In vivo antitumor effect of the DOX-ALG NPs against saline, empty ALG NPs and free DOX. *$P < 0.05$ since the seventh day, and **$P < 0.01$ since the seventh day.

seen that the H22 tumor grew rather fast for the groups administrated with saline and empty ALG NPs, and the average tumor volume in these two groups increases about 16-fold at day 15 compared to that at day 1. Compared with the control groups (saline and empty ALG NPs groups), the growth rate of tumor in free DOX group reduces in the initial 5 day after injection, but is accelerated later followed in the same pace of control groups. At 15 day postinjection, the tumor average volume of free DOX group is 12-fold over that at day 1. On the other hand, the tumor growth of the DOX-ALG NPs groups is significantly suppressed. At day 15, the average tumor volume of the DOX-ALG NPs group increases about 3 fold compared to that at day 1. These results indicate that DOX-ALG NPs inhibit tumor growth much more efficiently than free DOX formulation.

From Figure 8, it can also be seen that the antitumor efficacy of free DOX is valid in the initial 5 days, but seems to expire afterward. Probably, the DOX is cleaned up from the tumor. On the other hand, the antitumor effect of the DOX-ALG NPs lasts longer than free DOX. The tumors in the DOX-ALG NPs groups after day 11 are still effectively suppressed. This is most likely ascribed to the long blood circulation time and continued-DOX-release properties as well as long action time in tumor for the DOX-ALG NPs.

The survival rates of the mice in *in vivo* antitumor experiment are summarized in Figure 9, from which it can be seen that half of the mice in the control groups die within 15 days and all do not survive in 30 days because of fast growth of the H22 tumor. Also, the lifetime of the group that received free DOX is elongated by only a few days compared to that of control groups. On the other hand, the group treated with the DOX-ALG NPs receives the longest survival period in the experiments. Half of the mice survive more than 45 days, 3 mice stand to 59 days, and one mouse survive 63 days, because of the significant antitumor efficacy of the DOX-ALG NPs.

DOX Distribution In vivo. To gain a deeper insight into the in vivo behavior of these DOX-ALG NPs, and to better elucidate the reasons why DOX-loaded NPs have superior antitumor efficacy than free DOX, a biodistribution examination was conducted after i.v. injecting the DOX-ALG NPs at a DOX dose of 4 mg/kg, and free DOX at a DOX dose of 4 mg/kg for comparison. The distribution profiles of DOX in various tissues at different time points are displayed in Figure 10. It is

dx.doi.org/10.1021/am3012627 | ACS Appl. Mater. Interfaces 2012, 4, 5325−5332

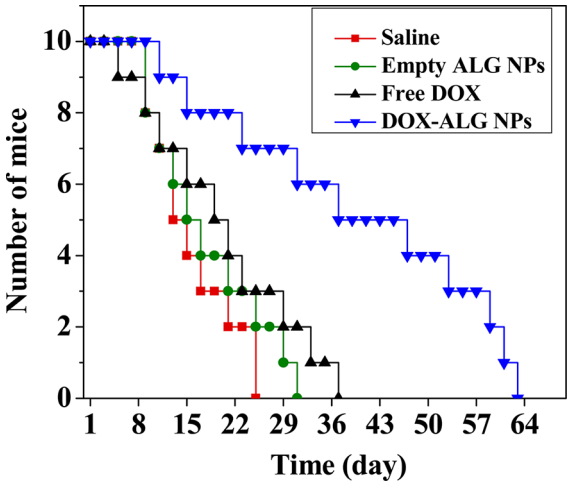

Figure 9. Suvival cure of the mice in the in vivo antitumor experiments.

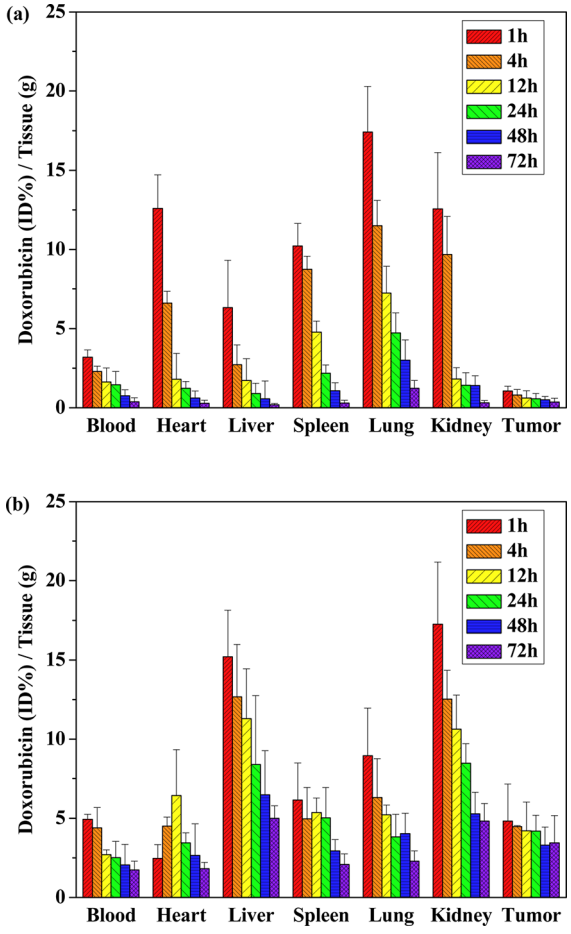

Figure 10. Biodistribution of (a) free DOX and (b) the DOX-ALG NPs.

found that the DOX level in blood for the DOX-ALG NPs (Figure 10b) is higher than that of free DOX (Figure 10a) at the same sampling time, indicating that the decay of DOX concentration in blood for free drug is very rapid and the circulation time of the DOX-ALG-NPs is much longer than free DOX. The DOX concentration in heart for free drug during 4 h postinjection is much higher than that of nanoparticle formulation. Thus, the ALG NPs can significantly reduce the cardiotoxicity of DOX. Meanwhile, the ALG NPs also decreases the DOX level in the lung compared with free DOX, which might depress the damage to the lung and increase its biosafety. From Figure 10b, it can be seen that the DOX accumulations in the liver and the kidney are significant, implying that some of DOX-ALG NPs are captured by liver and easy to be metabolized, which are in agreement with NIR fluorescence observation.

The DOX concentration in the tumor is also shown in Figure 10. From Figure 10b, it can be seen that the DOX concentration in tumor reaches its maximum in the initial 1 h after injection, that is, 4.8% ID (injected dose)/g tissue, and maintains (around 4.2% ID/g) within 24 h postinjection. After that, a decrease in DOX concentration in tumor is observed at 48 h after injection, but it remains 3.3% ID/g until 72 h postinjection. The DOX level in tumor for DOX-ALG NPs formulation is much higher than that for free DOX at each sampling time and lasts for a long period of 72 h at a relatively high level of 3.3% ID/g. There are some differences between this result and in vivo NIR fluorescence imaging (Figure 7) where the ALG NPs show apparent EPR accumulation to the tumor site after 4 h postinjection, whereas biodistribution reveals that the DOX level of the tumor reaches its maximum within 1 h. This is due to that in vivo NIR fluorescence imaging reflects the accumulation contrast of the nanoparticles in tumor and other organs, while the biodistribution determines the DOX level in the tumor. Thus, the biodistribution examination suggests that the ALG nanoparticlular formulation has a quick EPR accumulation and can make DOX stay in tumor for longer action time with relatively higher DOX concentration, improving the efficacy of drug-loaded nanoparticles in impeding tumor growth and prolonging the lifetime of tumor-bearing mice.

In addition, the DOX level in heart and lung of the mice received DOX-ALG NPs is significantly lower than that of free DOX, which is in agreement with some literatures reported.[37−40] Thus, the ALG NPs could significantly reduce the cardiotoxicity and damage to the lung of DOX.

CONCLUSIONS

In this work, a kind of novel ALG NPs was successfully prepared through nonsolvent-aided counterion complexation. The mean size of the ALG NPs obtained is about 100 nm with narrow size distribution. When these ALG NPs are used as DOX carriers, high DOX loading content (24.5%) and encapsulation efficiency (95.5%) are achieved, and a pH sensitive DOX release pattern from ALG NPs is observed. These negatively charged ALG NPs can be internalized well by the cancer cells through endocytosis fashion. In vitro cytotoxicity test reveals that the DOX-loaded ALG NPs have a similar cytotoxicity to free DOX at same DOX concentration. The in vivo real-time fluorescent imaging reveals that the ALG NPs can accumulate at tumor site via the blood circulation in tumor-bearing mice. In vivo antitumor efficacy examination exhibits that DOX-loaded ALG NPs have significantly superior antitumor effect compared to free DOX.

AUTHOR INFORMATION

Corresponding Author

*E-mail: jiangx@nju.edu.cn.

Notes

The authors declare no competing financial interest.

■ ACKNOWLEDGMENTS

This study was supported by the Natural Science Foundation of China (51033002, 20874042)

■ REFERENCES

(1) Brannon-Peppas, L. *Int. J. Pharm.* **1995**, *116*, 1.
(2) Song, C. X.; Labhasetwar, V.; Murphy, H.; Qu, X.; Humphrey, W. R.; Shebuski, R. J.; Levy, R. J. *J. Controlled Release* **1997**, *43*, 197.
(3) Soppimath, K. S.; Aminabhavi, T. M.; Kulkarni, A. R.; Rudzinski, W. E. *J. Controlled Release* **2001**, *70*, 1.
(4) Hans, M. L.; Lowman, A. M. *Curr. Opin. Solid State Mater. Sci.* **2002**, *6*, 319.
(5) Panyam, J.; Labhasetwar, V. *Adv. Drug Delivery Rev.* **2003**, *55*, 329.
(6) Wang, J. P.; Yoshie, M.; Kozo, T.; Tsuneji, N. *Int. J. Pharm.* **2000**, *203*, 61.
(7) Wong, H. L.; Rauth, A. M.; Bendayan, R.; Wu, X. Y. *Eur. J. Pharm. Biopharm.* **2007**, *65*, 300.
(8) Na, K.; Lee, T. B.; Park, K. H.; Shin, E. K.; Lee, Y. B.; Choi, H. K. *Eur. J. Pharm. Sci.* **2003**, *18*, 165.
(9) Song, C.; Labhasetwar, V.; Cui, X.; Underwood, T.; Levy, R. J. *J. Controlled Release* **1998**, *54*, 201.
(10) Tanaka, T.; Shiramoto, S.; Miyashita, M.; Fujishima, Y.; Kaneo, Y. *Int. J. Pharm.* **2004**, *277*, 39.
(11) Maeda, H. *Adv. Enzyme Regul.* **2001**, *41*, 189.
(12) Iyer, A. K.; Khaled, G.; Fang, J.; Maeda, H. *Drug Discovery Today* **2006**, *11*, 812.
(13) Muggia, F. M. *Clin. Cancer Res.* **1999**, *5*, 7.
(14) Leroux, J. C.; Allémann, E.; Jaeghere, F. D.; Doelker, E.; Gurny, R. *J. Controlled Release* **1996**, *39*, 339.
(15) Kong, G.; Braun, R. D.; Dewhirst, M. W. *Cancer Res.* **2000**, *60*, 4440.
(16) Luc, B.; Philippe, M.; Emilienne, S.; Lydie, L.; Sylviane, G.; Michèle, C.; Catherine, D.; Patrick, C.; Christian, T.; Ludmila, V. *J. Hepatol.* **2005**, *42*, 736.
(17) Rytting, E.; Bur, M.; Cartier, R.; Bouyssou, T.; Wang, X. Y.; Krüger, M.; Lehr, C.; Kissel, T. *J. Controlled Release* **2010**, *141*, 101.
(18) Dash, P. R.; Read, M. L.; Barrett, L. B.; Wolfert, M. A.; Seymour, L. W. *Gene Ther.* **1999**, *6*, 643.
(19) Kolambkar, Y. M.; Dupont, K. M.; Boerckel, J. D.; Huebsch, N.; Mooney, D. J.; Hutmacher, D. W.; Guldberg, R. E. *Biomaterials* **2011**, *32*, 65.
(20) Lee, J.; Tan, C. Y.; Lee, S. K.; Kim, Y. H.; Lee, K. Y. *J. Controlled Release* **2009**, *137*, 196.
(21) Hwang, Y. S.; Cho, J.; Tay, F.; Heng, J. Y.; Ho, R. S.; Kazarian, G.; Williams, D. R.; Boccaccini, A. R.; Polak, J. M.; Mantalaris, A. *Biomaterials* **2009**, *30*, 499.
(22) Yu, J. S.; Du, K. T.; Fang, Q. Z.; Gu, Y. P.; Mihardja, S. S.; Sievers, R. E.; Wu, J. C.; Lee, R. J. *Biomaterials* **2010**, *31*, 7012.
(23) Rajaonarivony, M.; Vauthier, C.; Couarraze, G.; Puisieux, F.; Couvreur, P. *J. Pharm. Sci.* **1993**, *82*, 912.
(24) Wang, T.; He, N. Y. *Nanoscale* **2010**, *2*, 230.
(25) Nanjwade, B. K.; Singh, J.; Parikh, K. A.; Manvi, F. V. *Int. J. Pharm.* **2010**, *385*, 176.
(26) Zhao, Q. H.; Han, B. S.; Wang, Z. H.; Gao, C. Y.; Peng, C. H.; Shen, J. C. *Nanomed.: Nanotechnol. Biol. Med.* **2007**, *3*, 63.
(27) Nesamony, J.; Singh, P. R.; Nada, S. E.; Shah, Z. A.; Kolling, W. M. *J. Pharm. Sci.* **2012**, *101*, 2177.
(28) Guo, R.; Zhang, L. Y.; Jiang, Z. P.; Cao, Y.; Ding, Y.; Jiang, X. Q. *Biomacromolecules* **2007**, *8*, 843.
(29) Rytting, E.; Bur, M.; Cartier, R.; Bouyssou, T.; Wang, X. Y.; Krüger, M.; Lehr, C.; Kissel, T. *J. Controlled Release* **2010**, *141*, 101.
(30) Dash, P. R.; Read, M. L.; Barrett, L. B.; Wolfert, M. A.; Seymour, L. W. *Gene Ther.* **1999**, *6*, 643.
(31) Patnaik, S.; Aggarwal, A.; Nimesh, S.; Goel, A.; Ganguli, M.; Saini, N.; Singh, Y.; Gupta, K. C. *J. Controlled Release* **2006**, *114*, 398.
(32) Gheorghe, F.; Elisabetta, E.; Doina, M.; Adrian, C.; Jacques, D.; Marguerite, R.; Claudio, N. *Int. J. Pharm.* **1998**, *170*, 11.
(33) Stubbs, M.; McSheehy, P. M. J.; Griffiths, J. R.; Bashford, C. L. *Mol. Med. Today* **2000**, *6*, 15.
(34) Gerweck, L. E.; Seetharaman, K. *Cancer Res.* **1996**, *56*, 1194.
(35) Hoesa, C. J. T.; Grootoonka, J.; Duncanb, R.; Humeb, I. C.; Bhakoob, M.; Boumac, J. M. W. *J. Controlled Release* **1993**, *23*, 37.
(36) Alexander, L. M.; Pernagallo, S.; Livigni, A.; Sanchez-Martın, R. M.; Brickman, J. M.; Bradley, M. *Mol. BioSyst.* **2010**, *6*, 399.
(37) Han, H. D.; Lee, A.; Song, C. K.; Hwang, T.; Seong, H.; Lee, C. O.; Shin, B. C. *Int. J. Pharm.* **2006**, *313*, 181.
(38) Cao, N.; Feng, S. S. *Biomaterials* **2008**, *29*, 3856.
(39) Kim, D.; Gao, Z. G.; Lee, E. S.; Bae, Y. H. *Mol. Pharm.* **2009**, *6*, 1353.
(40) Lu, D. X.; Liang, J.; Fan, Y. J.; Gu, Z. W.; Zhang, X. D. *Adv. Eng. Mater.* **2010**, *12*, 496.